Immunity, Vol. 10, 75–82, January, 1999, Copyright ©1999 by Cell Press

Structure of CD94 Reveals a Novel C-Type Lectin Fold: Implications for the NK Cell–Associated CD94/NKG2 Receptors

Jeffrey C. Boyington,* Aisha N. Riaz,* Apisit Patamawenu,* John E. Coligan,† Andrew G. Brooks,* and Peter D. Sun*‡
*Structural Biology Section
Office of the Scientific Director
†Laboratory of Immunogenetics
National Institute of Allergy and Infectious Diseases
National Institutes of Health
12441 Parklawn Drive
Rockville, Maryland 20852

Summary

The crystal structure of the extracellular domain of CD94, a component of the CD94/NKG2 NK cell receptor, has been determined to 2.6 Å resolution, revealing a unique variation of the C-type lectin fold. In this variation, the second α helix, corresponding to residues 102–112, is replaced by a loop, the putative carbohydrate-binding site is significantly altered, and the Ca^{2+}-binding site appears nonfunctional. This structure may serve as a prototype for other NK cell receptors such as Ly-49, NKR-P1, and CD69. The CD94 dimer observed in the crystal has an extensive hydrophobic interface that stabilizes the loop conformation of residues 102–112. The formation of this dimer reveals a putative ligand-binding region for HLA-E and suggests how NKG2 interacts with CD94.

Introduction

As an integral component of the innate immune system, NK cells are lymphocytes that participate in cytokine production and cytotoxicity. NK cell activity is tightly regulated by several families of receptors that recognize class I major histocompatability complex (MHC) molecules on the surface of target cells (reviewed by Long and Wagtmann, 1997; Moretta and Moretta, 1997; Lanier, 1998). These receptors effectively enable NK cells to discriminate between healthy cells and pathogen-infected cells or tumor cells by monitoring the levels of MHC class I molecules. Downregulation of MHC class I molecule expression through infections, tumorgenesis, or other cellular incursions may render cells susceptible to attack by NK cells (Ljunggren and Kärre, 1990; Pende et al., 1998). Structurally, these class I–recognizing receptors belong to either the immunoglobulin (Ig) superfamily (e.g., the killer cell inhibitory receptor [KIR] family) as type I transmembrane glycoproteins with one or more extracellular Ig domains or to the C-type lectin superfamily (e.g., CD94/NKG2 or Ly49) as dimeric type II transmembrane glycoproteins with a C-type lectin domain on the C-terminal of each chain. Both superfamilies include activating and inhibitory receptors. Inhibitory receptors contain cytoplasmic immunoreceptor tyrosine-based inhibitory motifs (ITIMs), while activating receptors possess a positively charged residue within the transmembrane region that interacts with an immunoreceptor tyrosine-based activation motif (ITAM)-containing adaptor molecule such as DAP12 (Lanier et al., 1998a, 1998b; Smith et al., 1998).

The CD94/NKG2 receptors are a family of heterodimeric proteins expressed on the surface of NK cells, with each comprised of an invariant CD94 polypeptide disulfide linked to either NKG2A/B, -C, or -E (Aramburo et al., 1990; Lazetic et al., 1996; Brooks et al., 1997; Carretero et al., 1997; Cantoni et al., 1998). NKG2A and -B are inhibitory and NKG2C and -E are activating. Recently, the ligand for the CD94/NKG2A/B and -C receptors has been identified as the nonclassical class Ib human leukocyte antigen (HLA)-E (Borrego et al., 1998; Braud et al., 1998; Lee et al., 1998), which presents peptides derived from the signal sequences of many HLA-A, -B, -C and -G alleles (Braud et al., 1997a). Cell surface HLA-E expression depends on the presence of these signal peptides, thus allowing for a rather elegant NK cell immunosurveillance strategy where nonpolymorphic CD94/NKG2 receptors are capable of monitoring the expression of the polymorphic class I MHC molecules through interaction with HLA-E (Braud et al., 1997a, 1997b).

Historically, C-type lectins have been defined as a superfamily of homologous modular carbohydrate recognition domains (CRD) of 115–130 residues that bind carbohydrate moieties in a Ca^{2+}-dependent manner and contain either two or three invariant disulfide bonds (short- and long-form C-type lectins, respectively) (Drickamer, 1993; Day, 1994). However, not all proteins characterized in this superfamily have been shown to bind carbohydrate (Day, 1994). The 200 or more protein sequences now known to contain C-type lectin domains are formally classified into seven different categories according to sequence homology and/or the overall modular architecture of the protein (Drickamer, 1993). CD94/NKG2 and other cell surface receptors such as Ly-49, NKR-P1, and CD69 form a unique category of C-type lectins, known as group V, which are distinctly different in sequence from the other categories. These dimeric receptors lack most of the conserved Ca^{2+}-binding residues observed in the majority of other sequences (Drickamer, 1993), and it has been suggested that they be renamed as a new family, the C-type lectin-like NK receptor domains (NKD) (Weis et al., 1998).

In contrast to the KIR receptors whose functional binding region has been mapped by mutagenesis and is supported by two crystal structures (Fan et al., 1997; unpublished data), very little is known regarding the structure of the NKD receptors, how they recognize their ligands, or how they dimerize. Moreover, there are no known structures of protein-binding dimeric cell surface receptors in the C-type lectin superfamily available to date. In an attempt to understand how this fold functions as a receptor to recognize protein ligands, we have determined the crystal structure of the ligand-binding domain of CD94.

‡To whom correspondence should be addressed (e-mail: sun@magenta.niaid.nih.gov).

Table 1. Data Collection, Phasing, and Refinement Statistics

Data Set	d_{min} (Å)	Unique Reflections	Redundancy	Completeness (%)	R_{sym}[c]	Sites (N)	Phasing Power[d]
Native[a]	2.6	6450	4.8	94.5	6.3	—	—
$AuCl_3$[b]	3.2	3626	6.1	99.1	7.2	3	2.81
K_2PtCl_4[b]	3.4	3109	4.6	98.8	9.2	10	0.95
UO_2 (oAc)[b]	4.0	1452	1.9	74.7	8.9	2	0.56
$IrCl_6$[b]	3.3	3331	5.9	98.5	7.0	6	0.98

Refinement (8.0–2.6 Å)

R_{cryst}	R_{free}[e]	Non-H Atoms	Solvent Sites	Rms Deviations	
				Bonds (Å)	Angles (°)
22.0	32.3	1036	39	0.009	1.6

[a] Data collected at the X9B beamline of the National Synchrotron Light Source (NSLS), Brookhaven, NY.
[b] Data collected on an R-AXIS IIC system (Molecular Structure Corporation).
[c] $R_{sym} = 100 \times \Sigma|I_h - <I_h>|/\Sigma I_h$, where $<I_h>$ is the mean intensity of multiple measurements of symmetry related reflections.
[d] Phasing power is the rms value of F_h divided by the rms lack-of-closure error. The overall figure of merit is 0.70–3.2 Å.
[e] R_{free} was calculated using 5% of the data.

Results and Discussion

The Overall Structure of CD94

The extracellular ligand-binding domain of human CD94, corresponding to residues 34–179, was expressed in a bacterial expression system and refolded in vitro. The crystal structure of this fragment was determined to 2.6 Å resolution by multiple isomorphous replacement and anomalous scattering (MIRAS) using four heavy atom derivatives (Table 1). The $2F_{obs}-F_{calc}$ electron density for CD94 forms a continuous map with no breaks, with the exception of N-terminal residues from the neck region. The final model comprises residues Cys59 to Ile179 (the numbering is consistent with the mature protein sequence). The molecule, with overall dimensions of approximately $42 \times 37 \times 33$ Å, consists of a three stranded antiparallel β sheet (strands 1, 2, and 7), a four stranded antiparallel β sheet (strands 4, 3, 5, and 6) and an α helix after strand 2 (Figures 1A and 1B). There are four intrachain disulfide bonds in CD94, three of which are the characteristic invariant disulfides (Cys61–Cys72, Cys89–Cys174, and Cys152–Cys166) found in long-form C-type lectins (Day, 1994). The fourth disulfide, Cys59–Cys70, which forms a looped structure with N-terminal β strands, is unique to the structure of CD94. The only extracellular cysteine not involved in intrachain disulfide pairing, Cys58, is expected to pair with the equivalent cysteine of NKG2 (e.g., Cys116 in NKG2A) to form the interchain disulfide in the CD94/NKG2 heterodimer.

Unlike the canonical C-type lectin fold, CD94 lacks one of two major α helices present in all other C-type lectin structures known to date. Specifically, the region from residues 102 to 112 (within loop 3), corresponding to the second helix of the consensus C-type lectin fold, adopts a loop conformation in CD94 (Figures 2A and 2C). The loss of this helix is unexpected considering the strong sequence similarity for this region with other lectins of known structure. However, CD94 has the shortest sequence in this region, with a 1–7 residue deletion near the C-terminal end of this loop relative to the other C-type lectins of known structure, which may contribute to the absence of this α helix. The conformation of loop 3 is stabilized by several nonpolar residues (Leu105, Phe107, Met108, and Tyr115) packing into a hydrophobic core, two salt bridges (Glu104–Lys175 and Asp106–Arg69), and several hydrogen bonds (Figure 2A). As a result of this helix-to-loop transformation, a neighboring hairpin loop (loop 6, residues 156–159) between β strands 5 and 6 moves into close contact with loop 3, making specific hydrogen bonds through the side chains of Asn156 and Asn158 and nonpolar interactions through Pro157.

The putative Ca^{2+}-dependent carbohydrate-binding loop (loop 5, residues 142–152) is 2–5 residues shorter in CD94 compared to other C-type lectins of known structure and displays a markedly different conformation as well as a different sequence (Figure 2B). Among the five consensus Ca^{2+} coordinating residues, only one is preserved in CD94 (Asp163, in β strand 6). Although residues Asn148 and Asn151 are in a position to be potential Ca^{2+} ligands, both side chains point away from the Ca^{2+}-binding site (Figure 2B). In contrast, the crystal structures of the known Ca^{2+}-dependent lectins and sequence alignments reveal a rather conserved Ca^{2+}-binding site (referred to as Ca^{2+} site 2 in rat mannose-binding protein [MBP]-A) with four or five protein side chains coordinating the calcium ion. Moreover, even the structure of human lithostathine (Brookhaven PDB entry 1LIT), which has no conserved Ca^{2+}-binding residues, has a loop 5 conformation very similar to those of the Ca^{2+}-dependent C-type lectins. Despite the fact that CD94 was crystallized in presence of 100 mM Ca^{2+}, no visible electron density can be attributed to bound Ca^{2+} in this vicinity. This is consistent with studies that show the binding of CD94/NKG2A/B and -C to HLA-E to be carbohydrate independent (Braud et al., 1998).

Apart from the missing helix and the conformation of the Ca^{2+}-binding loop, the rest of the CD94 structure is quite similar to the classical C-type lectin fold even though the average sequence identity is only 20% between CD94 and C-type lectins of known structure (Figure 2C). For example, a superposition of the core regions between the CD94 and rat MBP-A structures, excluding the missing helix and loop regions, results in a 1.2 Å root-mean-square (rms) deviation among 71 α carbons.

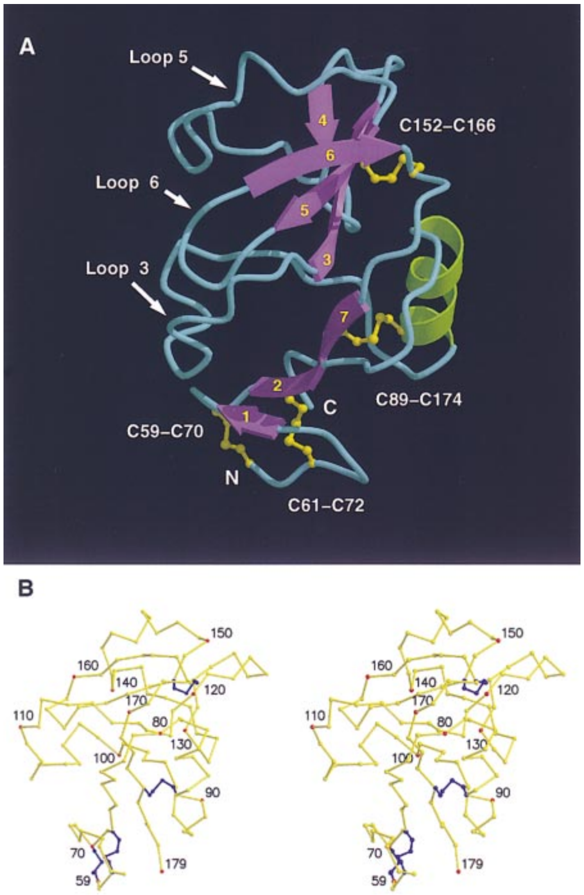

Figure 1. The Structure of Human CD94

(A) Ribbon diagram of the structure of CD94. β strands are shown in purple and are numbered according to their order in the sequence; the α helix is shown in green. The disulfide bonds are represented by yellow ball-and-stick models and labeled. Secondary structure assignments based on the program DSSP (Kabsch and Sander, 1983) are as follows: β strands 1–7 corresponding to residues 66–68, 71–75, 115–122, 127–129, 151–155, 161–165, and 171–176; α helix 1 corresponding to residues 82–91.

(B) Stereo view of an α carbon trace of CD94. Every tenth α carbon is colored red and labeled.

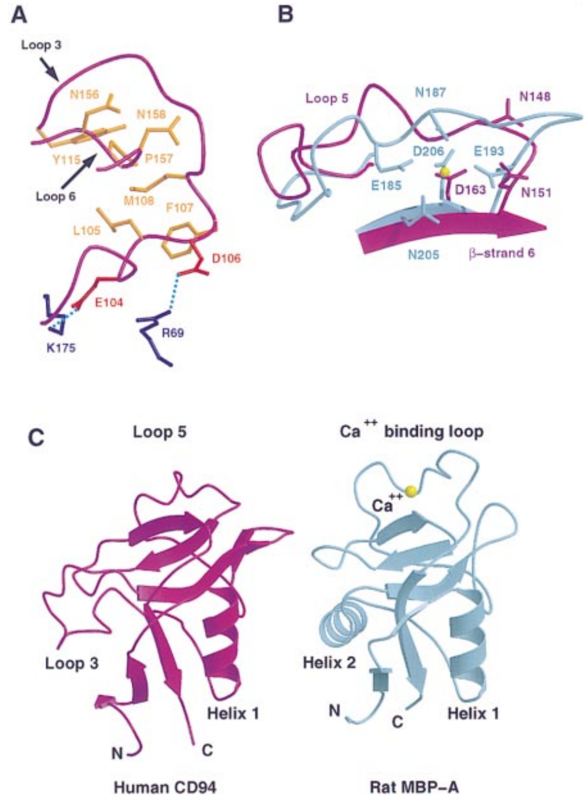

Figure 2. Comparison of Human CD94 and Rat MBP-A

CD94 is magenta and MBP-A (Brookhaven PDB entry 1RTM) is blue.

(A) Loops 3 and 6 in CD94. Side chains displayed are those that play a prominent role in stabilizing loop 3. Acidic residues are red, basic residues are blue, and neutral residues are tan. Two salt bridges are designated by dotted lines.

(B) Superposition of the Ca^{2+}-binding site of rat MBP-A with the same region in the human CD94 structure (loop 5 and β strand 6). Ca^{2+}-binding residues from MBP-A and potential Ca^{2+}-binding residues in CD94 are represented by ball-and-stick models.

(C) Superimposed and separated ribbon diagrams of the C-type lectin domains from CD94 (left) and MBP-A (right).

CD94 Exists as a Dimer with Extensive Interface Area

Functionally, CD94 exists in a heterodimeric disulfide-linked complex with NKG2A/B, -C, or -E (Aramburo et al., 1990; Lazetic et al., 1996; Brooks et al., 1997; Carretero et al., 1997; Cantoni et al., 1998). However, homodimeric CD94 has been found on the surface of certain transfected cell lines in which the expression of NKG2 is absent (Carretero et al., 1997; Lanier, 1998). Consistent with these observations, results from gel filtration and gel electrophoresis indicate that the extracellular portion of CD94 forms noncovalent dimers (data not shown). A 2-fold related crystallographic dimer was observed in CD94 crystals in which two monomers hydrogen bond through their respective first β strands, creating an extended six-stranded antiparallel β sheet (Figure 3). The interface of this elongated dimer is relatively flat and contains a central hydrophobic region (residues Val66, Tyr68, Ile75, Phe107, and Met108) (Figure 3) surrounded by hydrophilic residues with a buried surface area of 1204 Å^2, which is comparable to the interface area between the Vα and Vβ domains of the αβ T cell receptor (TCR) (Garboczi et al., 1996; Garcia et al., 1996). It is noteworthy that a significant part of the interface observed in this dimer involves loop 3, where the helix-to-loop transformation has occurred in CD94, suggesting that this loop conformation may be partly stabilized through hydrophobic interactions across the dimer interface.

Indeed, when loop 3 is modeled as an α helix into the CD94 dimer using the structural superposition of rat MBP-A and CD94 as a guide, it results in the C-terminal ends of the modeled helices packing loosely against each other at an angle of approximately 145°, creating steric hindrance with the existing loop 6. In addition, this results in a much smaller dimer interface, leaving several nonpolar side chains, including Val66, Tyr68, Ile75, Leu105 and Phe107 of CD94, solvent exposed. It thus appears that adopting a loop instead of a helical

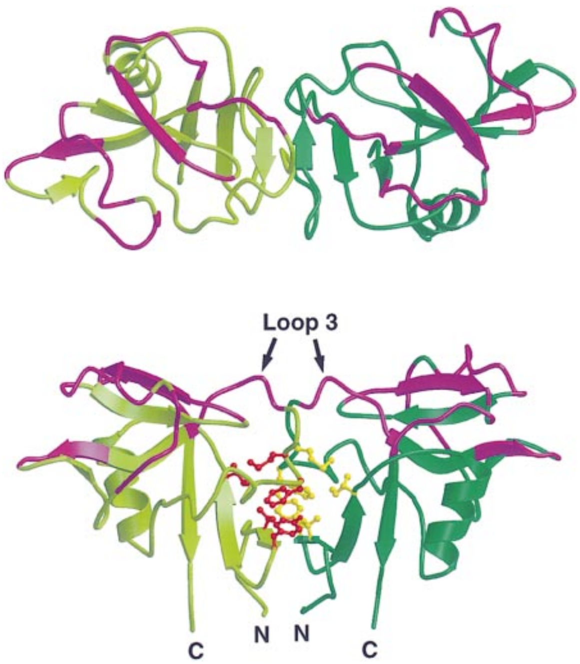

Figure 3. Ribbon Models Showing Two Views of the CD94 Dimer

Each monomer is colored a different shade of green. Regions that have low sequence identity with the NKG2 sequences are colored purple. The top view is rotated 90° from the bottom view along the horizontal axis. In the bottom view, residues in the hydrophobic core of the dimer interface (V66, Y68, I75, F107, and M108) are represented by ball-and-stick models. These residues are colored red in one monomer and yellow in the other.

conformation for residues 102–112 of CD94 helps to stabilize the dimer interface by burying hydrophobic side chains and increasing the dimer interface contact area.

The dimer arrangement observed in CD94 is unique among known structures of C-type lectin domains such as rat MBP-A and -C and human MBP, tetranectin, E-selectin and lithostathine, sea raven type II antifreeze protein, and the two subunits of heterodimeric snake venom coagulation factors IX/X-binding protein (Weis et al., 1991; Graves et al., 1994; Sheriff et al., 1994; Bertrand et al., 1996; Ng et al., 1996; Mizuno et al., 1997; Nielsen et al., 1997; Gronwald et al., 1998). Rat and human MBP and human tetranectin each form trimers that are held together by an N-terminal triple α helical coiled coil with limited contact between neighboring C-type lectin domains. The snake venom coagulation factors IX/X-binding protein is a disulfide-linked heterodimer of two C-type lectin domains that dimerize through an elongated loop between β strands 2 and 3 (Mizuno et al., 1997). This dimerization interface is on the opposite side of the domain compared to the dimerization interface of CD94. The C-type lectin domains of lithostathine and E-selectin are not known to form dimers. Though not physiological, crystallographic dimers are observed in two structures of rat MBP-A and -C, both of which are lacking their N-terminal trimerization domains. Albeit similar in buried surface area (1099 Å^2 and 1009 Å^2 for MBP-A and -C, respectively), these dimers have orientations significantly different from that observed in CD94.

The Dimer of CD94 Provides an Intriguing Model for the CD94/NKG2 Heterodimer

The primary sequences of NKG2 molecules A/B, C, and E share 27%–32% identity with CD94 within the C-type lectin domain with minimal insertions or deletions, suggesting a strong structural similarity between CD94 and the NKG2 molecules (Figure 4). The dimerization of CD94 brings the two N-terminal α carbons to within 7.4 Å of each other, which is consistent with having a disulfide bond between the two chains of the receptor. Modeling based on the CD94 homodimer structure reveals some interesting features about the putative CD94/NKG2 heterodimer interface. Of the five hydrophobic core residues at the dimer interface of CD94, three are completely conserved in the NKG2 sequences, and two are replaced with other nonpolar residues. This distinctly hydrophobic patch forms the largest contiguous nonpolar surface on both the CD94 monomer and the model of NKG2. While the CD94 homodimer has no interchain salt bridges, there are two potential regions of charge complementarity across the modeled CD94/NKG2 interface: one is between Asp106 of CD94 and Lys135 of NKG2A and the other is between Arg69 of CD94 and Glu122 of NKG2A. Lys135 and Glu122 are each conserved throughout NKG2A/B, -C, and -E sequences, but are replaced by Ser and Lys, respectively, in CD94, creating an unfavorable Arg69–Lys64 interaction across the CD94/CD94 interface. This may help to explain the favorable interaction between CD94 and NKG2 compared to CD94 homodimerization.

In order to form a heterodimer similar to the CD94 homodimer, NKG2 would be expected to have the same helix-to-loop transformation in the region between α helix 1 and β strand 3 as observed in CD94. Indeed, the sequence of loop 3 is remarkably homologous between CD94 and NKG2, with no insertions or deletions (Figure 4), and the NKG2 sequence is easily accommodated in the CD94 loop structure. In particular, among residues forming the hydrophobic core of loop 3, Phe107 is conserved in NKG2 sequences, Leu105 is replaced by methionine or isoleucine, and Met108 is replaced by a conserved leucine.

A fourth member of the NKG2 family, NKG2D, is significantly divergent. Although all nine NKG2 cysteines are conserved, NKG2D shares only 21% sequence homology with other NKG2 members, compared to 94%–95% sequence homology observed between the extracellular domains of NKG2A/B, -C, and -E (Houchins et al., 1991; Ho et al., 1998). Furthermore, no CD94/NKG2D heterodimers have been observed to date. Despite these differences, all five of the key hydrophobic residues facilitating dimerization of CD94 are also nonpolar in NKG2D. However, one other residue (Leu105) that forms part of the hydrophobic core stabilizing loop 3 in CD94 appears to be a deletion in NKG2D.

A Putative Binding Site for HLA-E

The areas of greatest sequence divergence between human CD94 and NKG2 occur outside the dimer interface in the C-terminal half of the molecule, forming a

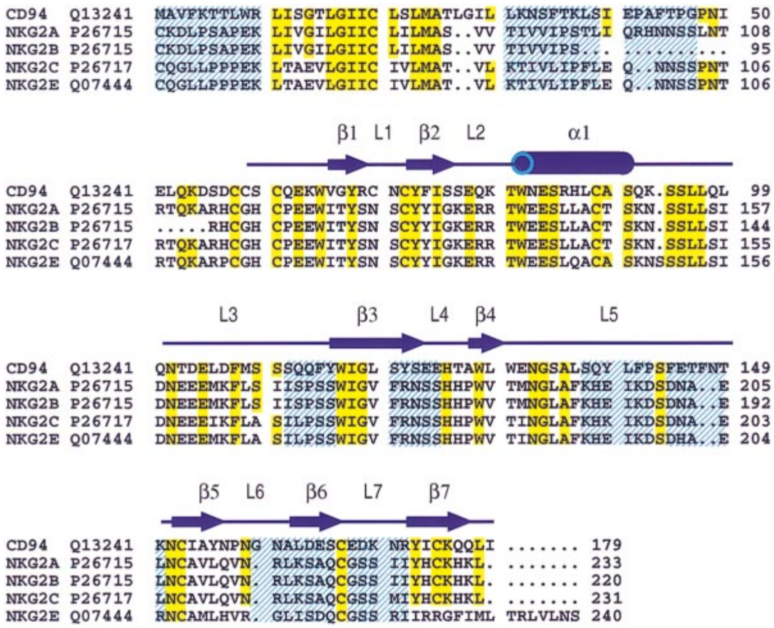

Figure 4. Sequence Alignment between Human CD94 and Human NKG2A/B, -C, and -E

The N-terminal cytoplasmic regions of NKG2A/B, -C, and -E that have no counterpart in CD94 are not shown. Swissprot accession numbers identify each sequence. Note that NKG2A and -B are likely different splicing products of the same gene (Houchins et al., 1991). The alignment was created using PILEUP from the GCG package (Wisconsin package version 9.0, Genetics computer group (GCG), Madison, Wisconsin) and edited by hand. Residues conserved with the CD94 sequence are highlighted in yellow. Regions of low sequence homology are highlighted by a blue hash. The secondary structure of CD94 is displayed above the alignment in blue. β strands and α helices in the CD94 structure are represented by arrows and cylinders, respectively.

contiguous surface at one end of the CD94 molecule (Figures 3 and 4). These variable regions, which encompass 2558 Å^2 of solvent-accessible surface area per monomer, abut each other to form a flat, uninterrupted surface across one face of the molecule opposite from the N- and C-termini. Based on this structure and sequence alignments, we postulate that the putative ligand-binding site resides within this variable region including residues 110–115, 120–124, 137–142, 144–150, 159–165, and 167–171 of human CD94 and the equivalent residues of human NKG2. The relative flatness of this putative binding region superficially resembles that of the MHC-binding surface observed on the αβ TCR (Garboczi et al., 1996; Garcia et al., 1996), in contrast to the well-carved binding surfaces of the human growth hormone receptor (De Vos et al., 1992). The variable region of CD94 has an overall net negative charge, with seven acidic residues and only three basic residues (Figure 5). In contrast, the corresponding regions of the NKG2A sequence is considerably more positively charged than CD94, with six basic residues and four acidic residues (Figure 5).

Loop 5 of CD94, corresponding to the Ca^{2+}-binding loop of the C-type lectin fold, is the longest of the putative HLA-E-binding loops. It is also the loop most different in sequence between CD94 and NKG2. In NKG2A, loop 5 is two residues shorter and contains seven out of the ten charged residues observed on the putative binding surface of NKG2 (compared to two out of the ten charged residues in the putative binding site of CD94). Since loop 5 is highly conserved between NKG2A/B, -C and -E, it may play a pivotal role in HLA-E binding.

Implications for the Structure of Other NK Cell Receptors of the C-type Lectin Superfamily

The crystal structure of CD94 provides a structural model for other group V C-type lectins, such as murine Ly-49A to -H, murine NKR-P1-2, -34, and −40, and both human and murine CD69, which are all distinctly different in sequence from other C-type lectins (references

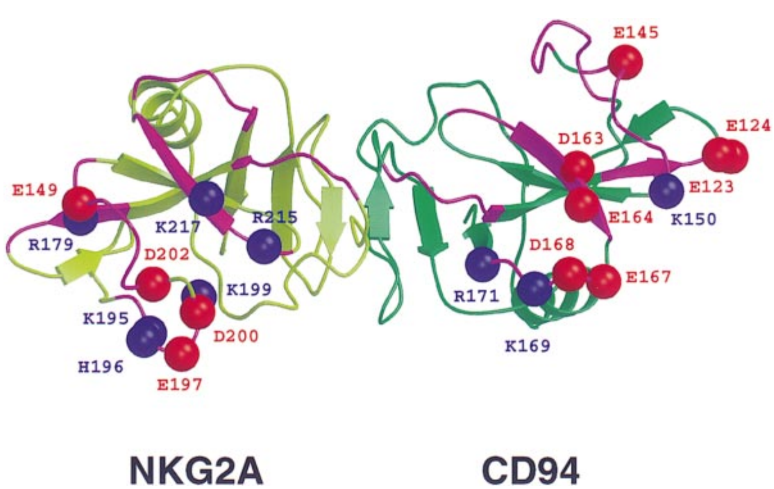

Figure 5. Model of the CD94/NKG2A Heterodimer

NKG2A is on the left side of the dimer represented by a light-green ribbon model and CD94 is on the right side represented by a dark-green ribbon model. Each of the charged residues within the putative HLA-E-binding surface is represented by a colored ball at the α carbon position and labeled according to the one-letter amino acid code. Red balls represent acidic residues and dark-blue balls represent basic residues.

for these sequences are found in Weis et al., 1998). The question remains as to whether or not these receptors dimerize in the same manner as CD94. The dimerization of CD94 is facilitated by a number of key hydrophobic residues (including Val66, Tyr68, Ile75, Leu105, Phe107, and Met108), by the unique conformation of loop 3, and by several hydrogen bonds. In both the Ly-49 and CD69 receptor families, all six of the nonpolar residues listed above are either conserved or replaced with other nonpolar residues, consistent with CD94 dimer formation. This is in contrast to the sequences of the known C-type lectin structures, which do not display a consistent sequence conservation of nonpolar residues at these six positions. In the murine NKR-P1 sequences, all but one of these residues (corresponding to position 68 in CD94) are nonpolar. The regions of the Ly-49, NKR-P1, and CD69 sequences corresponding to the dimer interface portion of loop 3, a key determinant in CD94 dimer formation, are rather conserved. However, the C-terminal region of this loop is 2–4 residues longer than in CD94 and displays considerable variability relative to CD94, NKG2, and to each other. Since the C-terminal end of loop 3 in CD94 and NKG2 may be involved in ligand binding, it is quite possible that these variable residues are also part of a binding loop.

Conclusions

Until now, information regarding the molecular details of the structure of the CD94/NKG2 family of receptors and how they interact with HLA-E (Figure 6) has remained elusive, despite the recent determination of the three-dimensional structure of HLA-E (O'Callaghan et al., 1998). The crystal structure of CD94 provides us with new insight regarding these questions. The structure reveals not only a novel variation of the canonical C-type lectin fold, but also a potential model for the CD94/NKG2 heterodimeric receptor. The sequences of NKG2A/B, -C, and -E each appear compatible with both the helix-to-loop transformation and the dimer interface. In addition, several key residues involved in CD94 dimerization are conserved in the sequences of Ly-49, NKR-P1, and CD69, suggesting the possibility that these receptors dimerize in a similar manner. We also propose a putative HLA-E-binding surface for CD94/NKG2 in which the NKG2 portion is predominately basic and the CD94 half is more acidic. However, the critical residues involved in ligand recognition remain to be proven by either analysis of mutations or the determination of structures of ligand receptor complexes.

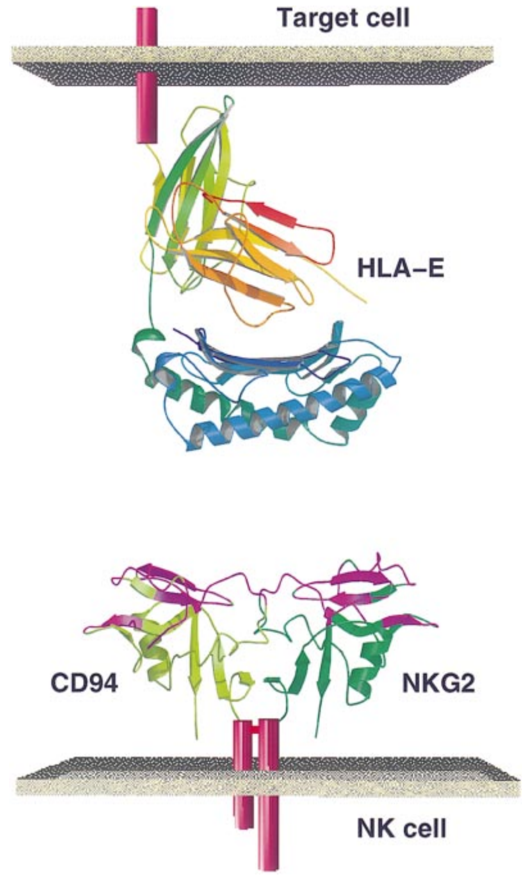

Figure 6. Hypothetical Model of the CD94/NKG2 Heterodimer and Its Ligand HLA-E on an NK Cell and a Target Cell, Respectively

The CD94/NKG2 heterodimer is represented by the CD94 homodimer. HLA-E coordinates were provided by C. O'Callaghan and J. Tormo. For greater clarity, the peptide bound to HLA-E is not shown.

Experimental Procedures

Protein Expression and Crystallization

The extracellular fragment of CD94 (residues 34–179) was expressed as inclusion bodies in *E. coli* BL21 cells and subsequently refolded by stepwise dilution and dialysis. After limited N-terminal proteolysis, crystals were grown by hanging drop vapor diffusion. Aliquots (1–5 μl) of CD94 (optical density at 280 nm = 16) were mixed with equal amounts of precipitation solution containing 15% PEG 8000, 100 mM $CaCl_2$, and 50 mM HEPES (pH 7.5) and suspended over a well containing 1.0 ml of precipitation solution. Elongated CD94 crystals grew to dimensions of $0.5 \times 0.15 \times 0.10$ mm within 2 weeks. The crystals belong to the hexagonal spacegroup $P6_522$ with cell dimensions of $a = b = 91.7$ Å, $c = 84.2$ Å and contain one molecule per asymmetric unit. Crystals were cryofrozen by step transfer to 20% glycerol in precipitation solution (increasing glycerol concentration by 5% every 30 min).

Structure Determination

All data were collected at −180°C. Diffraction data were processed using DENZO and SCALEPACK (Otwinowski and Minor, 1997) and scaled with CCP4 programs (CCP4, 1995). The major sites for the $AuCl_3$ derivatives were solved by inspection of difference Patterson maps. The other three derivatives were solved by difference Fourier methods. MLPHARE (CCP4, 1995) was used to generate and refine MIRAS phases from four heavy metal derivatives (Table 1). After subsequent phase improvement using DM (CCP4, 1995), the electron density map was readily interpretable. The model was built using O (Jones et al., 1991) and its positional and thermal parameters were refined by conjugate gradients using XPLOR 3.8 (Brünger, 1992). F_o's were scaled anisotropically during refinement to match F_c's, and a bulk solvent correction was applied.

Structural Analysis

Superposition of C-type lectin structures was performed using the program LSQMAN (Kleywegt and Jones, 1997). Solvent accessible surface area was determined using SURFACE with a 1.4 Å probe (CCP4, 1995). Modeling of the CD94/NKG2 heterodimer structure was performed by overlaying the sequence of NKG2A onto one monomer of the CD94 homodimer structure according to the alignment in Figure 4. The program O (Jones et al., 1991) was used to mutate side chains and to view the model. All figures except Figure 4 were produced with MOLSCRIPT (Kraulis, 1991) and RASTER3D (Merrit and Murphy, 1994).

Acknowledgments

We thank Z. Dauter and staff at NSLS beamline X9B and G. Snyder for help in synchrotron data collection; C. Hammer for mass spectroscopy; M. Garfield for amino acid sequencing; D. Garboczi, Y. Zhang, and D. Burshtyn for reviewing the manuscript; and C. O'Callaghan and J. Tormo for kindly providing coordinates for HLA-E.

Received September 25, 1998; revised December 14, 1998.

References

Aramburo, J., Balboa, M.A., Ramírez, A., Silva, A., Acevedo, A., Sánchez-Madrid, F., De Landázuri, M.O., and López-Botet, M. (1990). A novel functional cell surface dimer (Kp43) expressed by natural killer cells and T cell receptor-γ/δ^+ T lymphocytes. J. Immunol. *144*, 3238–3247.

Bertrand, J.A., Pignol, D., Bernard, J.-P., Verdier, J.-M., Dagorn, J.-C., and Fontecilla-Camps, J.C. (1996). Crystal structure of human lithostathine, the pancreatic inhibitor of stone formation. EMBO J. *15*, 2678–2684.

Borrego, F., Ulbrecht, M., Weiss, E.H., Coligan, J.E., and Brooks, A.G. (1998). Recognition of human histocompatibility leukocyte antigen (HLA)-E complexed with HLA class I signal sequence-derived peptides by CD94/NKG2 confers protection from natural killer cell-mediated lysis. J. Exp. Med. *187*, 813–818.

Braud, V., Jones, E.Y., and McMichael, A. (1997a). The human major histocompatibility complex class 1b molecules HLA-E binds signal sequence-derived peptides with primary anchor residues at positions 2 and 9. Eur. J. Immunol. *27*, 1164–1169.

Braud, V.M., Allan, D.S.J., Wilson, D., and McMichael, A.J. (1997b). TAP- and tapsasin-dependent HLA-E surface expression correlates with the binding of an MHC class I leader peptide. Curr. Biol. *8*, 1–10.

Braud, V.M., Allan, D.S.J., O'Callaghan, C.A., Söderström, K., D'Andrea, A., Ogg, G.S., Lazetic, S., Young, N.T., Bell, J.I., Phillips, J.H., et al. (1998). HLA-E binds to natural killer cell receptors CD94.NKG2A, B and C. Nature *391*, 795–799.

Brooks, A.G., Posch, P.E., Scorzelli, C.J., Borrego, F., and Coligan, J.E. (1997). NKG2A complexed with CD94 defines a novel inhibitory natural killer cell receptor. J. Exp. Med. *185*, 795–800.

Brünger, A.T. (1992). X-PLOR Version 3.1: a System for X-Ray Crystallography and NMR (New Haven, CT: Yale University Press).

Cantoni, C., Biassoni, R., Pende, D., Sivori, S., Accame, L., Pareti, L., Semenzato, G., Moretta, L., Moretta, A., and Bottino, C. (1998). The activating form of CD94 receptor complex: CD94 covalently associates with the Kp39 protein that represents the product of the NKG2-C gene. Eur. J. Immunol *28*, 327–338.

Carretero, M., Cantoni, C., Bellón, T., Bottino, C., Biassoni, R., Rodríguez, A., Pérez-Villar, J.J., Moretta, L., Moretta, A., and López-Botet, M. (1997). The CD94 and NKG2-A C-type lectins covalently assemble to form a natural killer cell inhibitory receptor for MHC class I molecules. Eur. J. Immunol. *27*, 563–567.

CCP4 (1995). The SERC (UK) Collaborative Computing Project No. 4. The CCP4 suite: programs for protein crystallography. Acta Crystallogr. D. *50*, 760–763.

Day, A.J. (1994). The C-type carbohydrate recognition domain (CRD) superfamily. Biochem. Soc. Trans. *22*, 83–88.

De Vos, A.M., Ultsch, M., and Kossiakoff, A.A. (1992). Human growth hormone and extracellular domain of its receptor: crystal structure of the complex. Science *255*, 306–312.

Drickamer, K. (1993). Ca^{2+}-dependent carbohydrate-recognition domains in animal proteins. Curr. Opin. Struct. Biol. *3*, 393–400.

Fan, Q.R., Mosyak, L., Winter, C.C., Wagtmann, N., Long, E.O., and Wiley, D.C. (1997). Structure of the inhibitory receptor for human natural killer cells resembles haematopietic receptors. Nature *389*, 96–100.

Garboczi, D.N., Ghosh, P., Utz, U., Fan, Q.R., Biddison, W.E., and Wiley, D.C. (1996). Structure of the complex between human T-cell receptor, viral peptide and HLA-A2. Nature *384*, 134–141.

Garcia, K.C. Degano, M., Stanfield, R.L., Brunmark, A., Jackson, M.R., Peterson, P.A., Teyton, L., and Wilson, I.A. (1996). An $\alpha\beta$ T cell receptor structure at 2.5 Å and its orientation in the TCR-MHC complex. Science *274*, 209–219.

Graves, B.J., Crowther, R.L., Chandran, C., Rumberger, J.M., Li, S., Huang, K.-S., Presky, D.H., Familletti, P.C., Wolitzky, B.A., and Burns, D.K. (1994). Insight into E-selectin/ligand interaction from the crystal structure and mutagenesis of the lec/EGF domains. Nature *367*, 532–538.

Gronwald, W., Loewen, M.C., Lix, B., Daugulis, A.J., Sönnichsen, F.D., Davies, P.L., and Sykes, B.D. (1998). The solution structure of the type II antifreeze protein reveals a new member of the lectin family. Biochemistry *37*, 4712–4721.

Ho, E.L., Heusel, J.W., Brown, M.G., Matsumoto, K., Scalzo, A.A., and Yokoyama, W.M. (1998). Murine *Nkg2d* and *Cd94* are clustered within the natural killer complex and are expressed independently in natural killer cells. Proc. Natl. Acad. Sci. USA *95*, 6320–6325.

Houchins, J.P., Yabe, T., McSherry, C., and Bach, F.H. (1991). DNA sequence analysis of NKG2, a family of related cDNA clones encoding type II integral membrane proteins on human natural killer cells. J. Exp. Med. *173*, 1017–1020.

Jones, T.A., Zou, J.Y., Cowan, S.W., and Kjeldgaard, M. (1991). Improved methods for building protein models in electron denisty maps and the location of errors in the models. Acta Crystallogr. A. *47*, 110–119.

Kabsch, W., and Sander, C. (1983). Dictionary of protein secondary structure: pattern recognition of hydrogen-bonded and geometrical features. Biopolymers *22*, 2577–2637.

Kleywegt, G.J., and Jones, T.A. (1997). Detecting folding motifs and similarities in protein structures. Methods Enzymol. *277*, 525–545.

Kraulis, P.J. (1991). MOLSCRIPT: a program to produce both detailed and schematic plots of protein structures. J. Appl. Crystallogr. *24*, 946–950.

Lanier, L.L. (1998). NK cell receptors. Annu. Rev. Immunol. *16*, 359–393.

Lanier, L.L., Corliss, B.C., Wu, J., Leong, C., and Phillips, J.H. (1998a). Immunoreceptor DAP12 bearing a tyrosine-based activation motif is involved in activating NK cells. Nature *391*, 703–707.

Lanier, L.L., Corliss, B.C., Wu, J., and Phillips, J.H. (1998b). Association of DAP12 with activating CD94/NKG2C NK cell receptors. Immunity *8*, 693–701.

Lazetic, S., Chang, C., Houchins, J.P., Lanier, L.L., and Phillips, J.H. (1996). Human natural killer cell receptors involved in MHC class I recognition are disulfide-linked heterodimers of CD94 and NKG2 subunits. J. Immunol. *157*, 4741–4745.

Lee, N., Llano, M., Carretero, M., Ishitani, A., Navarro, F., López-Botet, M., and Geraghty, D.E. (1998). HLA-E is a major ligand for the natural killer inhibitory receptor CD94/NKG2A. Proc. Natl. Acad. Sci. USA *95*, 5199–5204.

Long, E.O., and Wagtmann, N. (1997). Natural killer cell receptors. Curr. Opin. Immunol. *9*, 344–350.

Ljunggren, H.-G., and Kärre, K. (1990). In search of the missing self. MHC molecules and NK cell recognition. Immunol. Today *11*, 237–244.

Merrit, E.A., and Murphy, M.E.P. (1994). Raster 3D Version 2.0: a program for photorealistic molecular graphics. Acta Crystallogr. D. *50*, 869–873.

Mizuno, H., Fujimoto, Z., Koizumi, M., Kano, H., Atoda, H., and Morita, T. (1997). Structure of coagulation factors IX/X-binding protein, a heterodimer of C-type lectin domains. Nat. Struct. Biol. *4*, 438–441.

Moretta, A., and Moretta, L. (1997). HLA class I specific inhibitory receptors. Curr. Opin. Immunol. *9*, 694–701.

Ng, K.K.-S., Drickamer, K., and Weise, W.I. (1996). Structural analysis of monosaccharide recognition by rat liver mannose-binding protein. J. Biol. Chem. *271*, 663–674.

Nielsen, B.B., Kastrup, J.S., Rasmussen, H., Holtet, T.L., Graversen, J.H., Etzerodt, M., Thøgersen, H.C., and Larsen, I.K. (1997). Crystal structure of tetranectin, a trimeric plasminogen-binding protein with an α-helical coiled coil. FEBS Lett. *412*, 388–396.

O'Callaghan, C.A., Tormo, J., Willcox, B.E., Braud, V.M., Jakobsen, B.K., Stuart, D.I., McMichael, A.J., Bell, J.I., and Jones, E.Y. (1998). Structural features impose tight binding specificity in the nonclassical MHC molecule HLA-E. Mol. Cell *1*, 531–541.

Otwinowski, Z., and Minor, W. (1997). Processing of X-ray diffraction data collected in oscillation mode. Methods Enzymol. *276*, 307–326.

Pende, D., Accame, L., Pareti, L., Mazzocchi, A., Moretta, A., Parmiani, G., and Moretta, L. (1998). The susceptibility to natural killer cell-mediated lysis of HLA class I-positive melanomas reflects the expression of insufficient amounts of different HLA class I alleles. Eur. J. Immunol. *28*, 2384–2394.

Sheriff, S., Chang, C.Y., and Ezekowitz, R.A.R. (1994). Human mannose binding protein carbohydrate recognition domain trimerizes through a triple alpha-helical coiled-coil. Nat. Struct. Biol. *1*, 789–794.

Smith, K.M., Wu, J., Bakker, A.B.H., Phillips, J.H., and Lanier, L.L. (1998). Ly-49D and LY-49H associate with mouse DAP12 and form activating receptors. J. Immunol. *161*, 7–10.

Weis, W.I., Kahn, R., Fourme, R., Drickamer, K., and Hendrickson, W.A. (1991). Structure of the Ca^{2+}-dependent lectin domain from a rat mannose-binding protein determined by MAD phasing. Science *254*, 1608–1615.

Weis, W.I., Taylor, M.E., and Drickamer, K. (1998). The C-type lectin superfamily. Immunol. Rev. *163*, 19–34.

Brookhaven Protein Data Bank ID Code

The CD94 coordinates have been deposited in the Brookhaven Protein Data Bank under code 1b6e.